

Mediterranean Balloon Experiment: ocean wind speed sensing from the stratosphere, using GPS reflections

Estel Cardellach^{a,*}, Giulio Ruffini^b, David Pino^a, Antonio Rius^a,
Attila Komjathy^{c,1}, James L. Garrison^d

^a*Institut d'Estudis Espacials de Catalunya (IEEC/CSIC), Ed. Nexus, Gran Capita 2-4, 08034 Barcelona, Spain*

^b*Starlab, Ed. Observatori Fabra, Muntanya del Tibidabo, Cami de l'Observatori s/n, 08035 Barcelona, Spain*

^c*CCAR/University of Colorado at Boulder, Boulder, CO 80309, USA*

^d*Purdue University, West Lafayette, IN 47907, USA*

Received 21 September 2001; received in revised form 6 September 2002; accepted 27 May 2003

Abstract

The MEditerranean Balloon EXperiment (MEBEX), conducted in August 99 from the middle–up stratosphere, was designed to assess the wind retrieval sensitivity of Global Navigation Satellite Systems Reflections (GNSSR) technology from high altitudes. Global Positioning System reflected signals (GPSR) collected at altitudes around 37 km with a dedicated receiver have been inverted to mean square slopes (MSS) of the sea surface and wind speeds. The theoretical tool to interpret the geophysical parameters was a bistatic model, which also depends on geometrical parameters. The results have been analyzed in terms of internal consistency, repeatability and geometry-dependent performance. In addition, wind velocities have been compared to independent measurements by QuikSCAT, TOPEX, ERS/RA and a Radio Sonde, with an agreement better than 2 m/s. A Numerical Weather Prediction Model (NWPM, the MM5 mesoscale forecast model) has also been used for comparison with varying results during the experiment. The conclusion of this study confirms the capability of high altitude GPSR/Delay-map receivers with low gain antennas to infer surface winds.

© 2003 Elsevier Inc. All rights reserved.

Keywords: Global Positioning System (GPS); Scatterometry; Oceanography; Bistatic radar

1. Introduction

The Global Navigation Satellite Systems Reflections (GNSSR) technology, an implementation of the Passive Reflectometry and Interferometry System (PARIS) concept, has emerged as a remote sensing tool of great potential, offering a wide range of applications. It is now thought that the bistatic scattering of reflected GNSS signals can provide measurements for the study of the ocean surface (altimetry, sea state, sea winds), the cryosphere, land dielectric prop-

erties (soil moisture) and the atmosphere. This concept was originally developed by [Martin-Neira \(1993\)](#) (the PARIS concept), focusing on altimetric applications. PARIS aims to take advantage of available simultaneous observations from multiple footprints where geophysical parameters can be obtained. The multi-static character of PARIS exploiting GNSS signal of opportunity improves the coverage of measurements with respect to the monostatic instruments. Moreover, it does not require an on board emitter system (already operational) but only the receiving equipment, which can be continuously “listening”. Scatterometric GPSR observations for sea roughness and wind retrieval were proposed by [Garrison and Katzberg \(1998\)](#), based on the relationship between the degradation of the reflected signal and the sea roughness state. Several experiments have been conducted to demonstrate the concept ([Garrison & Katzberg, 1998](#); [Komjathy, Zavorotny, Axelrad, Born, & Garrison, 2000](#); [Martin-Neira, Caparrini, Font-Rossello, Lannelongue, & Serra, 2001](#); [Rius, Aparicio, Cardellach,](#)

* Corresponding author. Present address: NASA/Jet Propulsion Laboratory 238-600, 4800 Oak Grove Drive, Pasadena, CA 91109, USA. Tel.: +1-818-393-9008; fax: +1-818-393-4965.

E-mail addresses: Estel.Cardellach@jpl.nasa.gov (E. Cardellach), giulio.ruffini@starlab.es (G. Ruffini), pino@ieec.fcr.es (D. Pino), rius@ieec.fcr.es (A. Rius), Attila.Komjathy@jpl.nasa.gov (A. Komjathy), jgarriso@ecn.purdue.edu (J.L. Garrison).

¹ Present address: NASA/Jet Propulsion Laboratory 238-600, 4800 Oak Grove Drive, Pasadena, CA 91109, USA.

Martin-Neira, & Chapron, 2002). In the work of Lowe et al. (2002), we find a description of how the first Global Positioning System (GPS) reflections from space were detected in (very limited) historical Shuttle SIR-C data sets, a finding contributing to the validation of fundamental aspects of reflection models. Even so, more detailed analysis of experimental data obtained at higher altitudes is still needed to prepare future space-borne GNSS bistatic scatterometric systems. We present here the analysis of an experimental campaign using a low gain GPS receiver system at 37 km of altitude (higher than any previous dedicated experiment) to study the potential of the technique to infer ocean surface wind speeds—an important test for future space use of the GNSSR concept.

2. Experiment and data set

MEBEX was the result of a IEEC/CSIC-NASA collaboration. The GPSR instrument, a receiver developed at NASA Goddard Space Flight Center (GSFC) (Garrison et al., 2000) was placed as a secondary payload in a ASI/INTA Transmediterranean Balloon Campaign. The scientific objective of GPSR–MEBEX was to measure sea surface characteristics through the analysis of GPS signals scattered from the surface of the Mediterranean Sea. The NASA GPS receiver recorded the GPS signal reflected from the ocean surface using a low gain (6 dB) nadir-oriented LHCP antenna, and it used a RCHP up-looking antenna to track the direct signal. This receiver was a delay mapping receiver, i.e., it outputs the power associated to the correlation function between the signal and its PRN replica at delays around those corresponding to the specular point. The shape of this power-delay function shall be called a *waveform* from here on.

The MEBEX launch took place at 20:22 UTC August 1999. Stratospheric winds drove the balloon westward,

crossing the Mediterranean from Sicily to Southern Spain bordering the African Coast. The flight maintained an altitude of 37–38 km approximately for 14 h, and entered Spanish mainland airspace on August 3rd at noon. The tracks defined by the locations of the reflections on the Earth surface and collected by the receiver are shown in Fig. 1.

The Delay Mapping receiver was programmed to sequentially operate in different modes, but the present paper focuses on the data acquired by the *Serial Delay Mapping Receiver mode* (SDMR). In this mode, the receiver collected waveforms from up to six satellites at a time, for both direct and reflected channels. Once four or more satellites were tracked through the direct part of the receiver, the receiver was able to predict their specular point positions (and thus their delay and frequency offsets) and automatically search for them in the reflected signal. The observables detected by the receiver, the waveforms, were 32-bin long, corresponding to 32 half-chip sampling, performed every 100 ms (we refer to *chip* as the unit of the PRN code unit, as explained in Section 3.1). SDMR data has a somewhat reduced signal to noise ratio because of the sequencing acquisition limitations on the number of power measurements available to average within a fixed output sample interval. The raw 10-Hz waveforms were passed through a running window average filter to be written on disk at 1 Hz. Garrison et al. (2000) provided a detailed description of the receiver.

3. Data processing

3.1. Expected performance

In the frame of the ESA contract *Utilization of Scatterometry Using Sources of Opportunity, OPPSCAT*, a waveform simulator has been implemented and the feasibility of

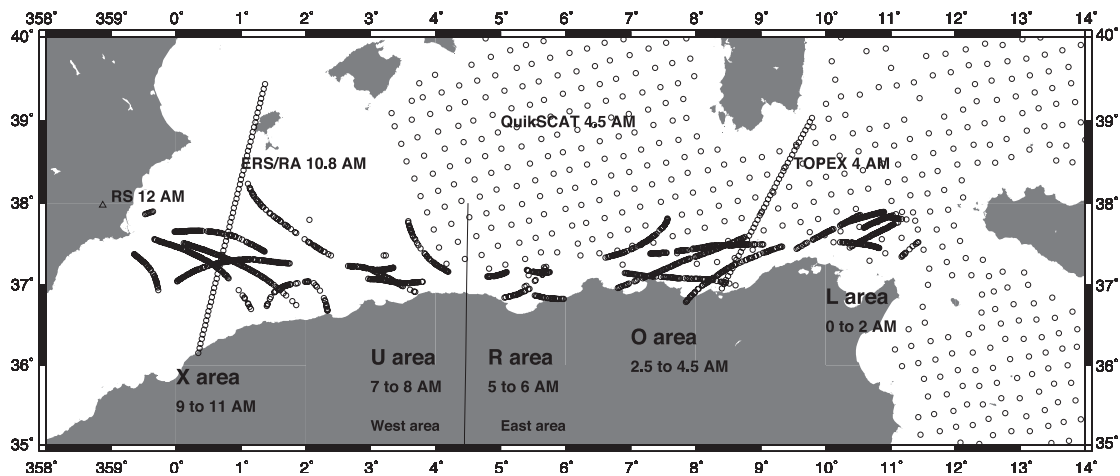


Fig. 1. Mediterranean Balloon Experiment crossing from Sicily to Spain. Tracks of the GPSR, QuikSCAT, ERS, TOPEX and Radio Sonde observation locations. Areas of GPSR measurements: L, O, R, U, and X. For MM5 comparisons, the data has been divided in two regions, East and West of longitude 4°:30'.

GNSS scatterometry has been analyzed (Cardellach & Ruffini, 2000). The simulator tool aims to reproduce the power associated to the correlation function of the reflected GPS signal (power waveforms) based on the models by Ruffini (1999) and Zavorotny and Voronovich (2000).

Three ideas lie behind the model.

- The reflected signal power has contributions from a certain area on the sea surface, the *glistening area*, the size and shape which depend on the roughness of the sea surface and the geometry of the reflection. The scattering coefficient from every patch on the sea surface is modeled as a function of the probability density function of the slopes of the sea surface facets. We have used the Kirchhoff electromagnetic approximation in its Geometric Optics approximation to compute the scattering coefficients. A Gaussian spectrum has been assumed, related to the wind speed through two different models by Apel (1994) and Elfouhaily, Chapron, Katsaros, and Vandemark (1997).
- The carrier has different Doppler frequency shifts depending on its path. This defines a set of strips or iso-Doppler contours over the sea surface. When tracking the signal, the receiver generates a signal with the Doppler of the specular point ray path, f_c (a receiver allowing sampling at multiple frequencies would be called a Delay-Doppler Mapping Receiver, instead of the Delay Mapping receiver used for MEBEX). The integration time filters out the signal with a frequency spread larger than $f_c \pm 1/T_i$. Thus, not the whole glistening is contributing to the acquired power, but just the fraction of the glistening area within the appropriate Doppler strip. This effect was not relevant in the MEBEX scenario, because the velocity of the receiver was slow enough to maintain the whole glistening in the first Doppler strip. Hence, there was no *Doppler filtering* in MEBEX data.
- Finally, the third idea behind the simulator is the delay filtering. The total amount of power from a certain transmitter arrives at the receiver with different time delays. This defines a set of iso-delay elliptical contours on the sea surface, *annuli* around the specular point. In order to isolate the transmitter signal from the rest of transmitters' signals, the incoming field must be cross-correlated with a clean replica of the emitted code (an orthogonal set of codes for the GPS constellation). The length of the code chip acts as a filter in the time domain through the correlation procedure. Hence, the correlation by a certain lag, t_{lag} , allows only power contribution from regions of the surface reflecting the signal with a delay within $[t_{lag} - 1 \text{ chip}, t_{lag} + 1 \text{ chip}]$. Thus, the power acquired per lag comes from reflections within the corresponding annulus on the sea surface: this is the concept of *delay mapping*.

The basic equation in the model, following the bistatic radar equation, is given in Eq. (1) for a given lag, τ and a

given frequency offset from the specular point, δf ($\delta f = 0$ in MEBEX receiver) (Ruffini, 1999):

$$SNR(\tau, \delta f) = \frac{P_t}{kTB_i} \int_{\text{sea surface}} \times d^2 \vec{\rho} \frac{G_t(\vec{\rho}) G_r(\vec{\rho}) \sigma^0(\vec{\rho}) A^2(\tau + \delta\tau(\vec{\rho})) |S(\delta f(\vec{\rho}))|^2}{(4\pi)^2 R_{(T, \vec{\rho})}^2 R_{(\vec{\rho}, R)}^2} \quad (1)$$

where P_t states for the transmitted power; kTB_i is the thermal noise after integration; $\vec{\rho}$ is the vector from the specular point to any other point on the sea surface; $R_{(T, \vec{\rho})}$ and $R_{(\vec{\rho}, R)}$ states for the distance from transmitter/receiver to any sea surface point $\vec{\rho}$ (part of the geometric power losses factor, jointly with $(4\pi)^2$); G_t and G_r are the antenna patterns (in the emitter/receiver system, respectively); σ^0 is the scattering coefficient; $|S(\delta f(\vec{\rho}))|^2$ is the expression for the Doppler filtering corresponding to $\vec{\rho}$; and $A(\tau + \delta\tau(\vec{\rho}))$ refers to its delay mapping attenuation.

The simulator was applied in two ways for the present MEBEX analysis: on the one hand, the tool itself was used to produce the residuals in the inversion procedure (Eq. (4)). On the other hand, the simulator was used to analyze the expected performance of the GPS reflection from a stratospheric balloon at 40 km of altitude (Cardellach & Ruffini, 2000). The study concluded that, because of the slow speed of a stratospheric balloon, the sensitivity to wind state was lower than for the same equipment boarded in an aircraft. The reduction of sensitivity was especially dramatic for the wind direction, formally impossible. The receiver on board of the stratospheric balloon had a very slow velocity (around 25 m/s) which poorly spreads the Doppler band width. This means that the whole glistening area is within the first iso-

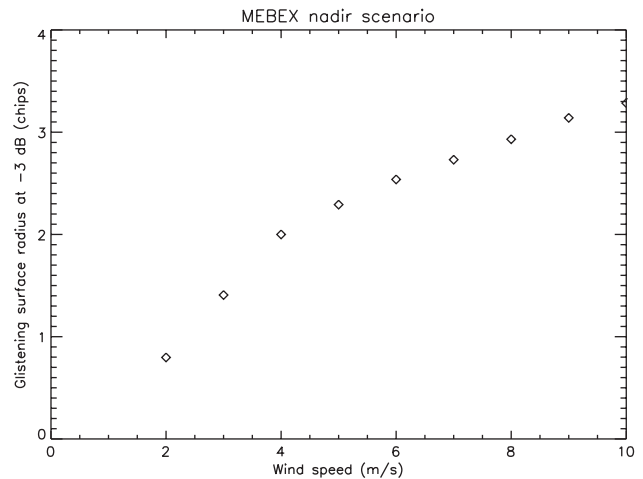


Fig. 2. Radius of the glistening surface in units of chips (nadir incidence case). The uncertainty of the wind retrieval is related with the variation of waveform shape, which is related to the energy redistribution when the glistening extends over a larger area. In the low wind range, the energy redistribution changes quicker when changing the wind conditions. When wind raises, the energy redistribution is so dependent on wind small variations. The conclusion is the loss of precision in the measurements when wind increases.

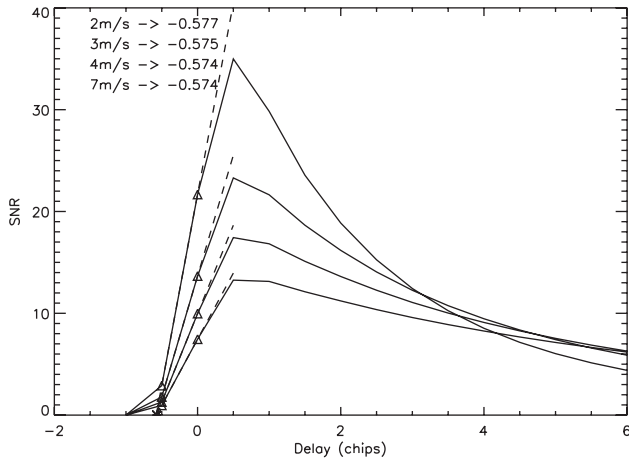


Fig. 3. Waveform alignment: modeled waveforms have a nearly invariant abscissa value for all linear fit computed with $\tau = -0.5$ chip and $\tau = 0$ chip. For simplicity, the real data has been aligned through a linear fit of $\tau_{\text{peak}} - 1$ and $\tau_{\text{peak}} - 0.5$ chips, and forced the crossing abscissa to the -0.57 chips value.

Doppler strip, independent of the different orientation of the glistening area, related to the wind direction. For this reason, the waveform samples the glistening area nearly in the same way, even for all wind orientations.

Wind intensity retrieval, however, appeared to be possible according to the performance analysis. Another conclusion from this analysis was that inversion suffers from a loss of precision of the measurement when the wind strength rises. The reason is that the variation in the waveform shape is related with the total energy redistribution as a function of the glistening area, with a nonlinear dependence of the wind speed. In the low winds range, the chip-measured size of the

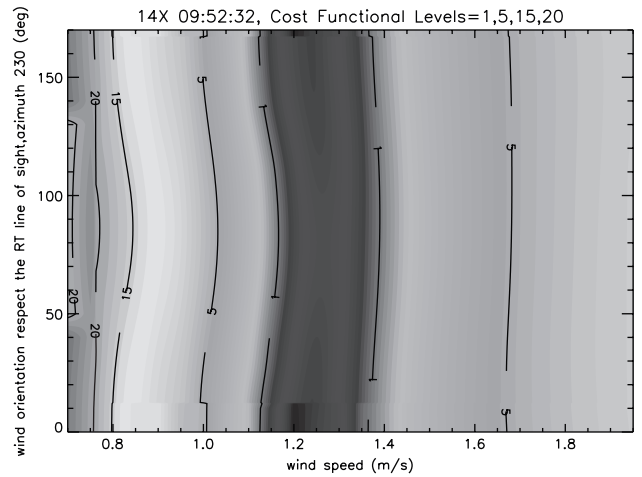


Fig. 5. Cost functional values for a single inversion of PRN 14 at X area. The cost functional contour plot shows a strong dependency on the wind speed, while the whole direction range lays inside the isoline-1, i.e. $\chi^2 \leq 1$. For cost functional values below 1, the uncertainty of the data and the mismodeling effects are greater than the post-fit residuals. Hence, the wind direction estimates have an uncertainty of 180° , not confident. For stronger winds, the width of this area in the wind speed axis raises due to the minor variation of the waveform shape.

glistening surface has a large variation for small wind perturbations. As wind grows up, the glistening area increases at a lower rate, and the energy redistribution also slows down, thus, it yields to less variation in the waveform shapes for a comparable change in wind speed. This concept is illustrated in Fig. 2, where the number of chips from where the power is scattered to the receiver is plotted as a function of the wind speed.

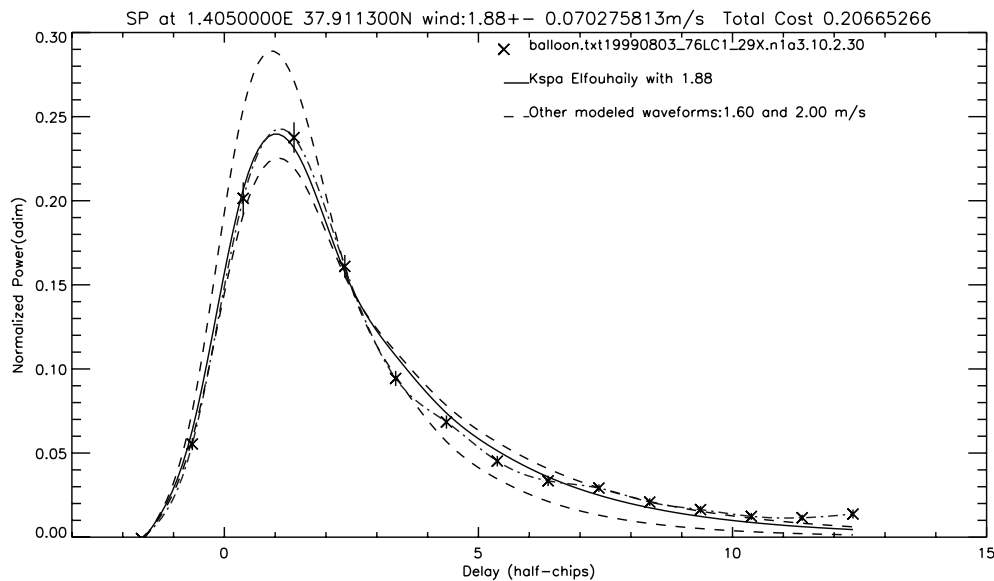


Fig. 4. An example of a waveform fit. Solid line: best fit waveform. Dash-dot line: split interpolation of the balloon's real data (crosses and bars). Dashed lines: modeled waveforms corresponding to wind speed off the solution. The trailing edge of 1-min averaged data oscillates between modeled waveforms corresponding to 2.0 and 1.6 m/s, while the covariance in these points is smaller than the oscillation itself (small error bars, not removable through averaging). This mismodeling effect is taken into account in the fit procedure.

3.2. Pre-processing

Before inversion, the waveform data was pre-processed in order to (a) reduce the noise, (b) align the delay offset and (c) remove uncalibrated power scaling factor effects.

3.2.1. Smoothing

The raw data at 1 Hz is too noisy to retrieve reliable wind estimates. Instead, 1-min averaging produced stable wave-

forms. The implemented smoothing procedure reduces each set of 61 raw waveforms to a single observation. In the MEBEX case, 1-min (or longer) incoherent averaging was permissible, given the very low speed of the balloon: spatial resolution was not affected (the receiver moved about 1.5 km during this time).

Another goal of pre-processing was to constrain the system to reduce the degrees of freedom in the inversion: the geophysical and instrumental parameters affecting the

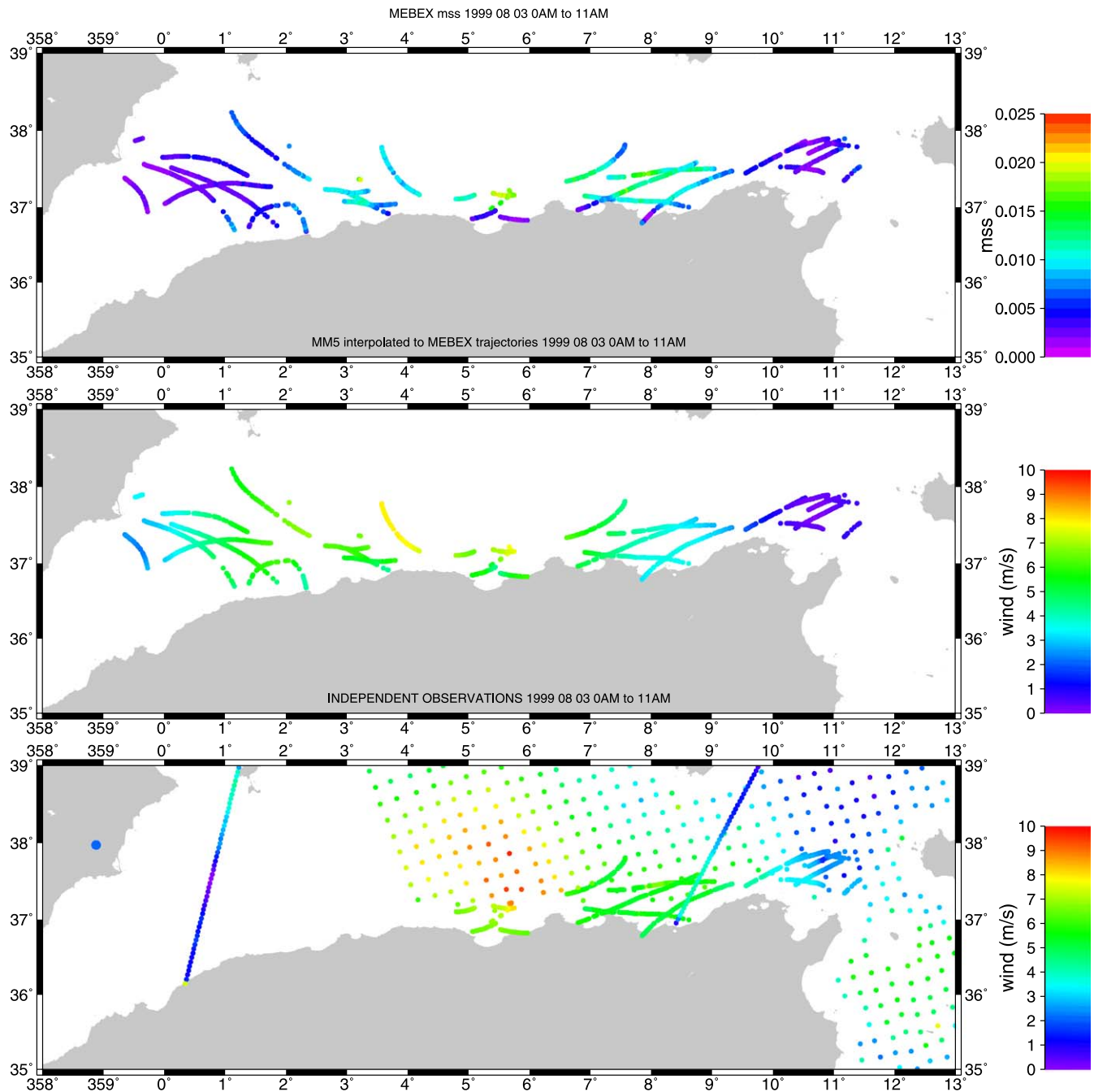


Fig. 6. (top) Map of the sea surface mean square slopes (MSS) obtained through the GPSR inversion. The Elfouhaily and Apel ocean models have been used to translate it to wind speed values (Figs. 10 and 12 show part of such models). (middle) MMS sea wind simulation interpolated, both in time and space, to MEBEX specular points' trajectories (color scale in m/s). (bottom) Independent observations: TOPEX and ERS/RA wind products, QuikSCAT interpolated to MEBEX arcs and Radio Sounding Balloon measurement (color scale in m/s).

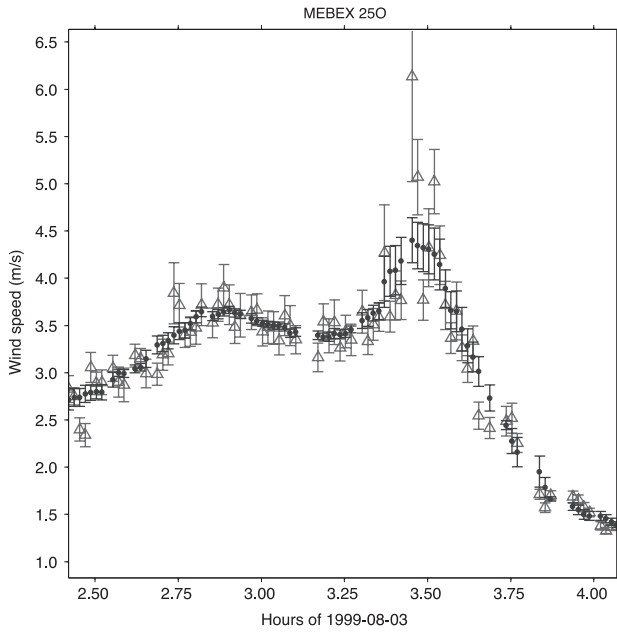


Fig. 7. Time series of a complete arc (PRN 25, area O). The triangles solution corresponds to the single inversions and their uncertainty, independent each one from the others (no filtering, no recursive a prioris). The circles and their bars are the 10-min-averaged smoothed solution and its dispersion (rms).

waveform are the wind vector (speed and direction), the delay offset (which introduces a misalignment in the time axis), and scaling factors arising from uncalibrated instrumental effects. The whole suite of parameters might be introduced into the estimation procedure, being treated as unknowns as done by Garrison, Komjathy, Zavorotny, and

Katzberg (2002). In the case presented here, the system becomes degenerate when optimizing a functional cost for more than two parameters and then, the solution is rather dependent on the a prioris. For these reasons, the delay and the power offsets have been removed prior to the optimization, in the pre-processing phase.

3.2.2. Delay alignment

The receiver computes the delay of each bin in terms of chip distance from the nominal specular point delay. However, this operation of the receiver is not calibrated, and misalignments can be introduced in the data, corrupting the inversion procedure by mismatched comparison with the models. The alignment requires the existence of an invariant point in the leading edge of the waveform, searched through the use of modeled waveforms. The leading edge of the waveform has been modeled for different wind states to find a common point. Fig. 3 shows an almost invariant point obtained by means of the first two half-chips of the map ($\tau = -0.5$ and $\tau = 0$ chips). In that case, the axis crossing point was located around -0.57 chips. The misalignment $\delta\tau$, the delay quantity to be shifted to obtain the abscissa crossing of the linear fit, was thus -0.57 chips. For simplicity, the linear fit has been computed with the samples: $\tau_{\text{peak}} - 1$ and $\tau_{\text{peak}} - 0.5$ chips, and the waveforms shifted to locate the crossing abscissa point at -0.57 chips.

3.2.3. Power scaling factor and offset

The power offset is directly related to the additive noise of the instrument (from both receiver and transmitter) and acquires different values for each transmitter–receiver link.

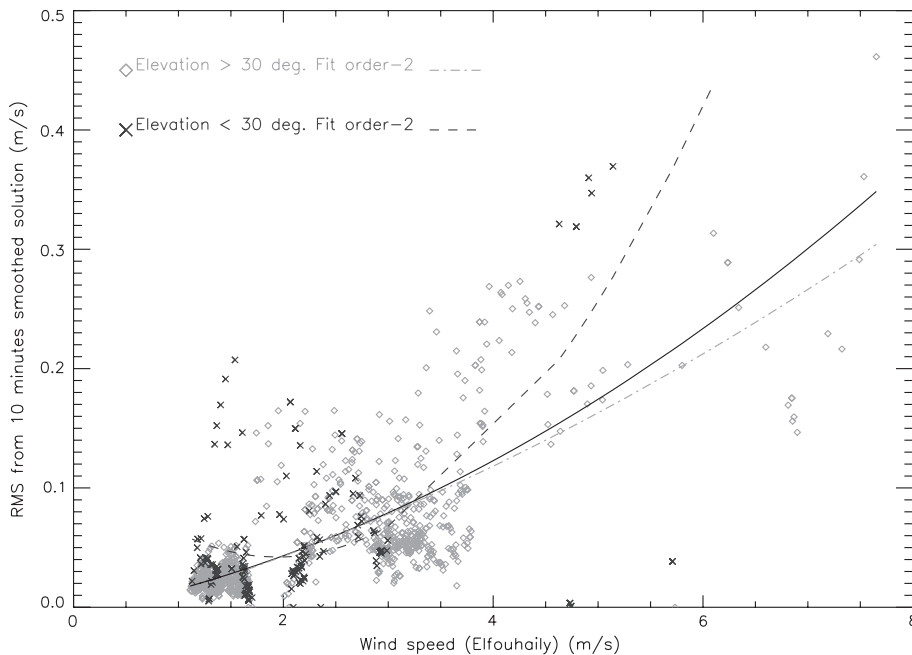


Fig. 8. rms of the time series points with respect to the 10-min smoothed solution. Light grey diamonds and dashed-dot fit line for GPSR observations with elevation above 30° , dark crosses and dashed fit line for elevation below 30° . Solid line for the global fit.

The approach we use treats all data before $\tau = -0.57$ chips as noise floor, and subtracts the mean power of all those data from the waveforms. On the other hand, the uncalibrated scaling factor effect is removed through a re-normalization of the waveform by its total energy (as described by Garrison et al., 2002; Komjathy et al., 2000).

3.3. From waveforms to wind speed: inversion procedure

The MEBEX waveforms were compared to modeled waveforms to obtain sea state information. The modeled waveform was a function of a model state \vec{m} , containing the model parameters such as wind stress and direction:

$$\vec{P}_{\text{mod}} = \vec{f}(\vec{m}) \tag{2}$$

To invert the power observations into wind/sea estimates, a nonlinear cost functional χ has been minimized:

$$\chi^2(\vec{m}) = \vec{r}^T(\vec{m}) \cdot W \cdot \vec{r}(\vec{m}) \tag{3}$$

where the residual \vec{r} is:

$$\vec{r}(\vec{m}) = \vec{P}_{\text{obs}} - \vec{P}_{\text{mod}}(\vec{m}) \tag{4}$$

being \vec{P} 1-min-averaged power-delay map, normalized by its total energy. The subindices obs and mod stand for balloon’s pre-processed data and modeled waveform, respectively.

The weighting coefficients given by the W matrix contain the inverse of the data covariance, C_d^{-1} and other factor

Table 1
Cross-over points analysis

SVs and area	Δt min	$\Delta \text{elev.}$ ($^\circ$)	w mean speed (m/s)	Δw (m/s)
05 24 L	23	25	1.42	0.11
06 08 L	20	13	1.21	0.01
29 30 L	37	34	1.36	0.39
06 25 O	22	14	3.24	0.49
17 30 O	24	15	3.13	0.26
17 25 O	19	20	2.27	0.28
03 21 U	8	13	2.51	0.07
21 31 U	26	9	2.99	0.20
01 03 X	5	2	1.59	0.20
01 31 X	14	15	1.46	0.14
14 31 X	26	4	1.32	0.09
Linear regression coefficient				
	0.006 (m/s)/min	0.005 (m/s)/deg	0.14 (m/s)/(m/s)	

The first column contains the Space Vehicle numbers which generated the cross-over point and the area of observation (see Fig. 1 to locate the areas). Columns 2 and 3 contain the delay and elevation difference between both observations. Column 4 is the mean of the inverted wind speed (using Elfouhaily’s model) and the last one contains the comparison offset. The mean agreement between cross-observations from different emitters of the same spot on the sea surface is 0.20 m/s. The regression coefficient from linear fits shows that the disagreement depends more strongly on wind speed than on Δt or $\Delta \text{elev.}$

derived from mismodeling. In a great part of the data set, the model had trouble to fit the trailing edge of the waveform, where systematic low variance oscillations are not removable through averaging (Fig. 4). This unmodeled effect has

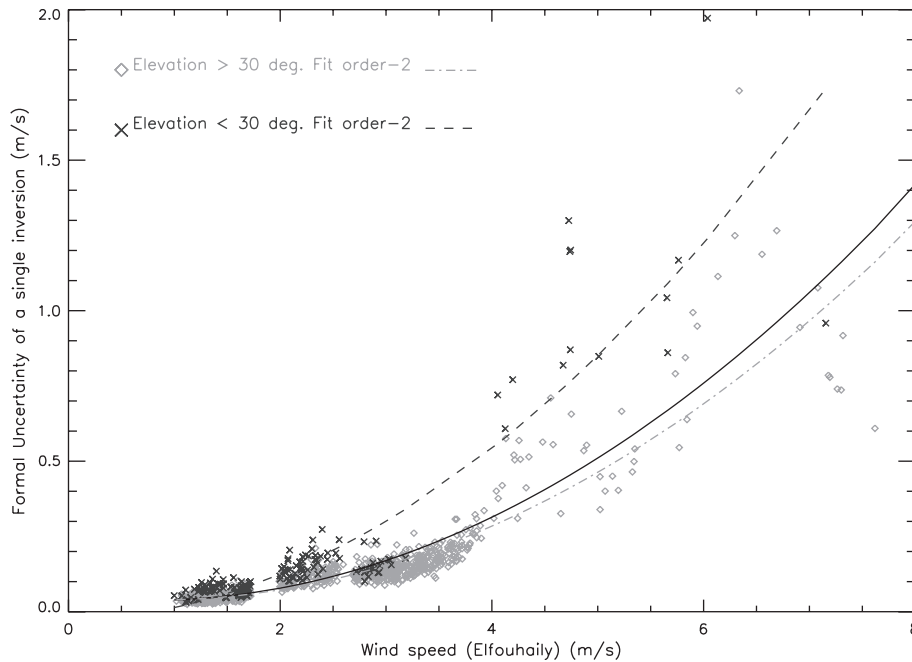


Fig. 9. Formal uncertainty of single inversions. It is related to the width of the area within the cost functional below 1 (Fig. 5), meaning that a wind speed variation around the solution drives to a fit where the post-fit residuals are of the same order than the data uncertainty and mismodeling. Light grey diamonds and dashed-dot fit line for GPSR observations with elevation above 30°, dark grey crosses and dashed fit line for elevation below 30°. Solid line for the global fit.

Table 2
Independent wind product sources and space and time coverage/sampling capabilities to be compared with MEBEX-GPSR data

Product	Spatial coverage	Time coverage	H_w
MEBEX	Different tracks, few kilometers wide, each one of variable length, up to 200 km	One inversion per minute, footprint at ~ 25 m/s of mean speed	10 m
Radio Sonde	Single point, closer GPSR at ~ 50 km	Single moment, simultaneous to some GPSR	59 m
TOPEX/GDR-M wind product	track few kilometers wide, 100 km off the simultaneous GPSR	Few seconds to cross the area, offset time >1 h from GPSR	10 m
ERS/RA/ATSR wind product	track few kilometers wide, 100 km off the simultaneous GPSR	Few seconds to cross the area, offset time ~ 1 h from GPSR, except few points at 0.5 h	10 m
QuikSCAT Level 2b	25×25 -km grid, 25 km off the Coast, where most GPSR were collected	Few minutes to cover the area, offset time ~ 15 min w.r.t. some GPSR measurements	10 m
MM5	15×15 -km grid, topography resolution: 5 km	grid output per hour	sea level

been included in the inversion at the weighting matrix, through a factor $p_{\text{lag}}/p_{\text{peak}}$:

$$W = [C^w]^{-1} \quad (5)$$

defining C^w as

$$C_{i,j}^w = C_{i,j}^d \cdot \frac{P_{\text{peak}}^2}{P_i \cdot P_j} \quad (6)$$

where C^d is the covariance of the 1-min-averaged balloon's data; $P_{\text{peak},i,j}$ are the power of the peak, the i -th and the j -th lag, respectively.

The complete solution is thus given by the model vector \vec{m}^* that minimizes the cost functional χ^2 , and the covariance matrix of this solution is C_M . The algorithm

selected to optimize the nonlinear system is the *Powell* method (Numerical Recipes), a direction set method in multi-dimension which does not require any explicit computation of the function's gradient. This algorithm does not store the solution's covariance matrix. For linear models, the formal uncertainty is defined as the width of the region in the model space where the probability of having the true estimate is greater than e^{-1} . In a linear and Gaussian system, this information lays on the diagonal elements of the solution covariance matrix, C_M (Tarantola, 1987):

$$C_M = [F^t \cdot C_w^{-1} \cdot F]^{-1} \quad (7)$$

where F is the linear operator of the model. For this nonlinear system, the computation of the formal uncer-

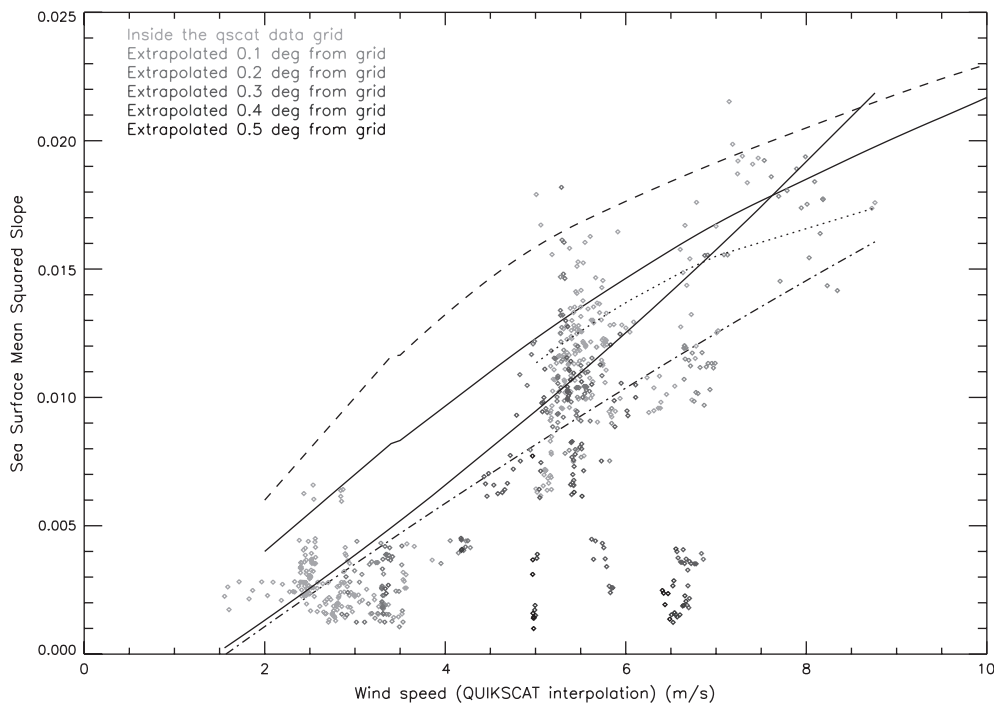


Fig. 10. Mean square slope of the sea surface from GPSR observations as function of QuikSCAT *ground truth*. Solid line: Apel's model. Dashed line: Elfouhaily's model. Dash-dot line: second order fit with all data set. Dash-dot-dot line: second order fit with GPSR observation inside the QuikSCAT grid. Dotted line: second order fit with GPSR observation inside the QuikSCAT grid and within 1 h of time offset from the QuikSCAT measurement.

tainty has been carried out through the linearized problem equations around the solution m^* , thus F in Eq. (7) becomes:

$$F \equiv \left(\frac{\delta f}{\delta m} \right) m = m^* \tag{8}$$

This was numerically computed.

4. Analysis and discussion

The goal of our analysis was the validation of the GPSR wind retrieval procedure from a receiver located in the mid-upper stratosphere. To this end, more than 1500 1-min-averaged waveforms collected in the MEBEX experiment have been inverted to wind velocity vectors. After removing outliers and bad inversions, the clean data set amounted to 1300 points, which have been analyzed in terms of repeatability, consistency, formal uncertainty and external comparisons. Wind direction estimates are left out from the analysis, since they are not reliable as described in Section 3.1, and shown in Fig. 5. The technique for wind direction retrieval proposed by Armatys, Komjathy, Axelrad, and Katzberg (2000), based on the coupled analysis of two-satellite footprints observing the same area from different incidence plan, has also failed under the available MEBEX geometrical conditions. Hence, we restrict the discussion to the wind speed results, as obtained from the mean square slopes (MSS) values in Fig. 6 (top) and Elfouhaily’s and Apel’s models. As described by Zavorotny (1999), MSS parameters can be related to the surface elevation spectrum (and hence, to a wind parameter) by appropriate integration over wavelengths longer than a two-scale dividing parameter. We emphasize that MSS is in fact the primary measurement of GPSR, wave spectrum and other models were used to produce comparison values for MSS as function of wind speed.

4.1. Repeatability, coherence and formal uncertainty

The wind speed results obtained through the MEBEX-GPSR data set were tested for self-consistency: repeatability, measured here as the root mean square (rms) of the time series with respect to its 10-min smoothed solution, has a mean value of 0.05 ± 0.06 m/s. Eighty-eight percent of the rms values were below 0.1 m/s. This is a good indicator, specially because each individual inversion in the time series is independent of the rest (neither Kalman filtering techniques nor recursive a prioris have been employed) while the footprints of consecutive waveforms overlap. An example is shown in Fig. 7.

One of the relevant new aspects introduced by the bistatic character of the GPSR is the dependence of its capabilities on the geometry of the reflection. The geometric parameter to consider in the wind speed inversion is the

elevation angle (defined as the angle between the horizon and the transmitter or receiver, from the specular point of view). According to our results, the effect of elevation in wind speed estimates repeatability is not as relevant as the wind dependency itself (Fig. 8). Moreover, this behavior also drives the formal uncertainty of the single inversions, strongly dependent on the wind intensity and secondarily dependent on the elevation (Fig. 9). We remark that no very low elevation (grazing angles) inversions have been included in the comparison, only four observations below 10 and 36 between 10° and 20° .

In order to check the internal consistency of the results, the repeatability from different transmitter signals must be also verified. To this end, the wind speed estimates obtained in the cross-over points of different PRN arcs have been compared. Only 12 cross-over points took place, one of them with a delay greater than 1 h which has not been analyzed. The rest have time offsets up to 37 min. Table 1 contains the cross-comparison values, with a mean agreement of 0.20 ± 0.14 m/s. As before, the impact of the elevation is not relevant—although no extreme cases were

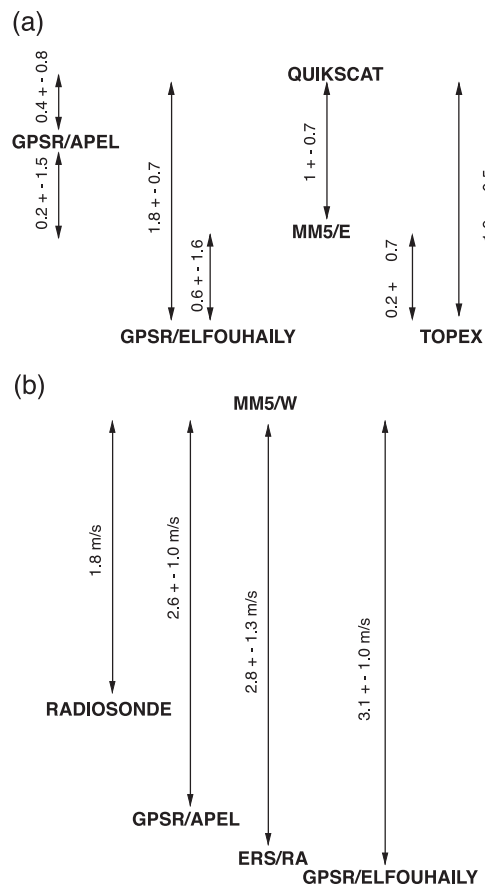


Fig. 11. Cross-comparison between independent sources of wind speed data, QuikSCAT overlap. (a) Eastern area, night observations, no QuikSCAT measurements. (b) Western area, day observations. The wind observations through Elfouhaily’s model have similar bias with respect to QuikSCAT and MM5 than the Radar Altimeter wind observations (TOPEX, ERS).

present—compared to the wind strength itself. The conclusion from the cross-over analysis corroborates the self-coherence of the estimates. However, repeatability and consistency would probably suffer under windier meteorological conditions, since these parameters seem to be driven by the wind speed.

4.2. External analysis: comparison with independent sources

A difficult aspect of comparing MEBEX results to other sources is the different space and time sampling (Fig. 1). Different remote sensing instruments provided comparison data in the region near the MEBEX trajectory during the mission. We had access to data coming from a Radio Sonda, QuikSCAT satellite scatterometer, TOPEX and ERS satellite Radar Altimeters (RA). Space–Time sampling comparison limitations are summarized in Table 2. In addition to observational data from these independent sources, comparisons have extended to the Pennsylvania State National Center for Atmospheric Research (PSU-NCAR) fifth generation Mesoscale Model (MM5) outputs.

QuikSCAT Level 2b wind products [*QuickSCAT User's Manual*] (Weiss, 2000) have been interpolated/extrapolated to the eastern MEBEX tracks' positions (Fig. 6, bottom). However, most of the GPSR observations have a large time offset with respect to the QuikSCAT over-pass (up to 4 h). The comparison yields different values when con-

sidering all the data set, when rejecting QuikSCAT grid outliers, or when selecting points according to a time offset criteria. Moreover, the choice in the ocean surface models (Apel, Elfouhaily) also had an impact on the comparisons. Restricting the comparison to GPSR observations located inside the QuikSCAT grid and within 1 h time offset yields a bias of 1.8 m/s (QuikSCAT higher winds) and a rms of 0.7 m/s (Elfouhaily's model). Using Apel's model, the bias reduces to 0.4 m/s with a bit more dispersion: 0.8 m/s of rms. Another way to visualize these discrepancies is through the plot in Fig. 10, which shows MEBEX MSS against QuikSCAT winds. The points far away from the ocean models are off the QuikSCAT grid, closer to the coast. On the other hand, the points selected for the comparison have a second order fit parallel to Elfouhaily's model and biased $\sim +2$ m/s, while the fit crosses Apel's function. The TOPEX GDR-M wind product (AVISO/Altimetry, 1996) from track 161 has been used for comparison with QuikSCAT wind velocities. TOPEX crossed the QuikSCAT area 30 min before, and the direct comparison gives an offset of 1.9 m/s, similar to QuikSCAT vs. GPSR with Elfouhaily mean value.

The other gridded data source available for interpolation to a great number of MEBEX locations is the MM5 Numerical Weather Prediction Model (NWPM) (Dudhia, 1993), whose initial and boundary conditions are updated every 6 h with information obtained from the $0.5^\circ \times 0.5^\circ$ ECMWF model. The MM5 simulation provides the sea surface wind at each point of the grid (15 km resolution)

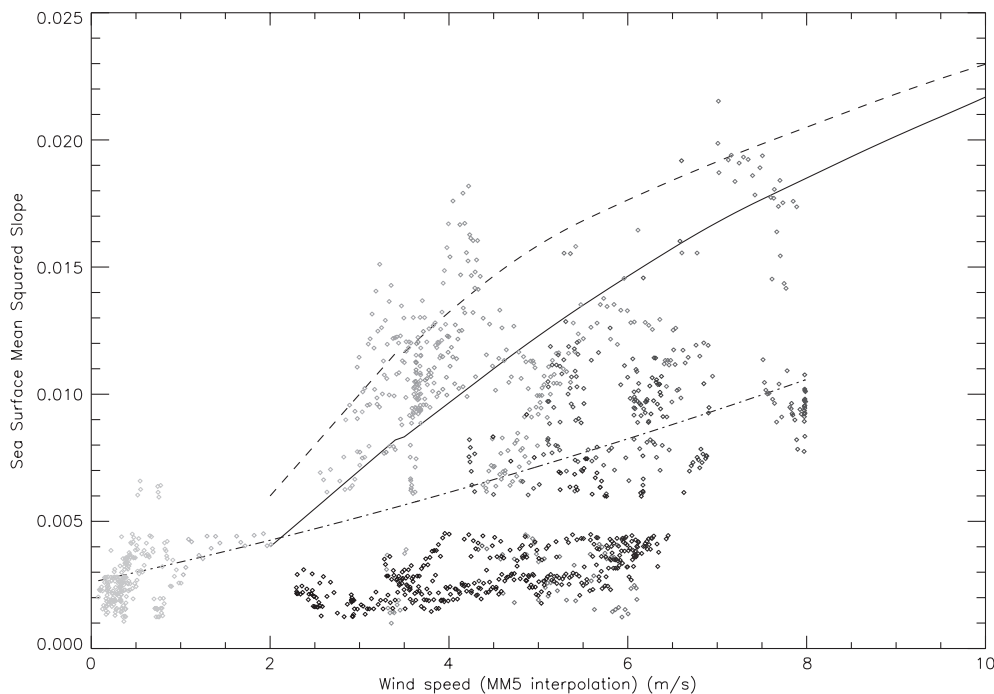


Fig. 12. Mean square slopes from GPSR observations as function of the MM5 *ground truth*. Grey scale corresponds to the time evolution of the experiment. Solid line: Apel's model. Dashed line: Elfouhaily's model. Upper dotted line: second order fit using East area measurements. Lower dotted line: second order fit using measurements from the Western area.

and every hour. This set of simulated data has been interpolated both in space and time to MEBEX specular point trajectories (Fig. 6, middle). We split the comparison in two different areas, corresponding to two different spatial domains defined in the simulation. Moreover, such division also corresponded to those MEBEX nocturne/daily observations and with/without QuikSCAT overlaps. The Eastern region (longitudes above 4.5° , with night MEBEX observations and QuikSCAT measurements) compares with GPSR as a small bias (<1 m/s) but large dispersion (>1.5 m/s), for both Elfouhaily and Apel models (Fig. 11a). On the contrary, the comparison in the western area yields a large bias but smaller dispersion ($\sim 3 \pm 1$ m/s). Visualized in terms of MSS as function of MM5 ground truth (Fig. 12), the points of the eastern comparison are mainly located around the theoretical models, whereas the western points are located far from the models, at high wind speeds. This raises the question of whether MM5 has a wrong wind estimation in this area or, on the contrary, GPSR is not sensitive to wind speed. In this sense, recent work (Pagowski & Moore, 2001) has showed the inconsistencies in the way that MM5 calculates surface fluxes over the ocean. This fact could explain why the comparisons in high convective situations, i.e., during the daytime, give a larger bias than at night. Moreover, comparing with the oceanic data of Wu (1969) and, as Bao, Wang, Wilczak, and Dudhia (1998) showed by means of a coupled ocean–wave–atmosphere model simulations, the way in which MM5 calculates the roughness over water presents some inaccuracies. Another possibility to explain the comparison results in the western area may be the insensitivity of GPSR under certain swell-wind conditions. No in situ records of swell have been found. The ERS/RA and the Radio Sonde observations cannot be directly compared to GPSR due to the different time–space sampling. Nevertheless, they both can be cross-compared through MM5. As showed in (Fig. 11b), the observational independent source biases with respect MM5 are closer to GPSR one. In any case, this does not answer the previous question because, on one hand, the Radio Sonde was over land, where the MM5 performance is different than over sea. On the other hand, it has been shown that wind products from Radar Altimetry may be also affected by the swell (Gourrion, Vandemark, Bailey, & Chapron, 2000), which might explain the similarity of GPSR and ERS/RA wind measurements. Both instruments are sensitive to the surface MSS, which is in fact the primary measurement of GPSR.

5. Conclusions

The GPSR MEditerranean Balloon EXperiment (MEBEX) was carried out in 1999 August 03/04 to obtain delay mapping observations from a dedicated GPSR receiver

at 37 km of altitude. The data, averaged at 1-min intervals, aligned in the time domain through a pre-processing technique and re-normalized by total energy, was then inverted to obtain surface roughness (MSS, the primary measurement). The MSS values were compared to surface wind speed predicted by several different models. The inversion procedure optimizes a nonlinear cost functional where the weighting matrix takes into account the data covariance and mismodeling.

After cleaning the data, the inferred wind speeds from 1300 1-min-averaged waveforms have been analyzed. The inferred orientation of the wind is not relevant, because of the low velocity of the receiver. On the contrary, repeatability and consistency of wind speed estimates appear to be much better than 1 m/s. However, this encouraging result is partially satisfying because of the low winds regime in effect during the experiment. As expected, the results corroborate a loss of precision in the measurements with increasing wind speeds.

Direct external validation with independent observational sources has only been possible with QuikSCAT. A comparison with a 74-sample set has resulted in a bias of 1.8 ± 0.7 m/s (QuikSCAT-GPSR/Elfouhaily). The rest of observational data (ERS/RA, TOPEX, Radio Sonde) have been cross-compared through the MM5 NWPM. Their wind estimates are coherent with GPSR, specially when using the Elfouhaily's model.

The experiment analysis highlights the potential of high altitude GPSR/Delay-map receivers with low gain antenna to infer sea surface roughness and, indirectly, the wind speed. It has validated the GPSR scatterometric concept and models for high altitude receivers and has provided an experimental basis for assessing potential future spaceborne applications.

Acknowledgements

Many thanks to all of the people that helped make possible this experiment: the ASI and INTA teams, the CSIC and NASA administrations. The research has been partially funded by ESA under OPPSCAT contract 13461/99/NL/GD AO/1-3478 (ESA Technical Manager: Pierluigi Silvestrin) and the Department of Presidency, Universities and Research, Generalitat de Catalunya. We would like to thank the GPSR team at CCAR/University of Colorado at Boulder, and Penina Axelrad for the technical discussions and Valery Zavorotny (CIRES/University of Colorado at Boulder/NOAA/ETL) for his contribution to the test of the forward model performance.

References

- Apel, J. R. (1994). An improved model of the ocean surface wave vector spectrum and its effects on radar backscatter. *Journal of Geophysical Research*, 99, 16269–16291.

- Armatys, M., Komjathy, A., Axelrad, P., & Katzberg, S. J. (2000, July). A comparison of GPS and scatterometer sensing of ocean wind speed and direction. *Proceedings of IGARSS 2000*.
- AVISO/Altimetry (1996). *AVISO User Handbook for Merged TOPEX/POSEIDON products*, AVI-NT-02-101, Edition 3.0.
- Bao, J. -W., Wang, W., Wilczak, J., & Dudhia, J. (1998). Numerical simulation of air–sea interaction under high wind conditions: A case study. *Preprints, 8th. PSU/NCAR Mesoscale Modeling System Users' Workshop* (pp. 22–26). Boulder, CO: NCAR.
- Cardellach, E., & Ruffini, G. (2000). *OPPSCAT WP3400: End-to-End Performance*, Final Report ESA Contract 13461/99/NL/GD.
- Dudhia, J. (1993). A nonhydrostatic version of the Penn-State-Ncar mesoscale model: Validation tests and simulation of an atlantic cyclone and cold front. *Monthly Weather Review*, *121*, 1493–1513.
- Elfouhaily, T., Chapron, B., Katsaros, K., & Vandemark, D. (1997). A unified directional spectrum for long and short wind-driven waves. *Journal of Geophysical Research*, *102*, 15781–15796.
- Garrison, J. L., Katzberg, S. J., & Hill, M. I. (1998). Effects of sea roughness on bistatically scattered range coded signals from the Global Positioning System. *Geophysical Research Letter*, *25*(13), 2257–2260.
- Garrison, J. L., Komjathy, A., Zavorotny, V., & Katzberg, S. (2002, January). Wind speed measurement using forward scattered GPS signals. *IEEE Transactions on Geoscience and Remote Sensing*, *40*(1), 50–65.
- Garrison, J. L., Ruffini, G., Rius, A., Cardellach, E., Masters, D., Armatys, M., & Zavorotny, V. U. (2000). Preliminary results from the GPSR mediterranean balloon experiment (GPSR–MEBEX). *Proceedings of ERIM 2000, Remote Sensing for Marine and Coastal Environments, Charleston, South Carolina, USA, 1–3 May*.
- Gourrion, J., Vandemark, D., Bailey, S., & Chapron, B. (2000, May). *Satellite altimeter models for surface wind speed developed using ocean satellite crossovers*, IFREMER-DROOS-2000-02.
- Komjathy, A., Zavorotny, V. U., Axelrad, P., Born, G. H., & Garrison, J. L. (2000). GPS signal scattering from sea surface: Comparison between experimental data and theoretical model. *Remote Sensing of Environment*, *73*, 162–174.
- Lowe, S. T., LaBrecque, J. L., Zuffada, C., Romans, L. J., Young, L. E., & Hajj, G. A. (2002). First spaceborne observation of Earth-reflected GPS signal. *Radio Science*, *37*, 1.
- Martin-Neira, M. (1993). A passive reflectometry and interferometry system (PARIS): Application to ocean altimetry. *ESA Journal*, *17*, 331–355.
- Martin-Neira, M., Caparrini, M., Font-Rossello, J., Lannelongue, S., & Serra, C. (2001, January). The PARIS concept: An experimental demonstration of sea surface altimetry using GPS reflected signals. *IEEE Transactions on Geoscience and Remote Sensing*, *39*(1), 142–150.
- Numerical Recipes in C: The Art of Scientific Computing*. Cambridge Univ. Press.
- Pagowski, M., & Moore, W. K. (2001, January). A numerical study of an extreme cold-air outbreak over the Labrador Sea: Sea ice, air–sea interaction, and development of polar lows. *Monthly Weather Review*, *129*, 47–72.
- Rius, A., Aparicio, J. M., Cardellach, E., Martín-Neira, M., & Chapron, B. (2002). Sea surface state measurements using GPS reflected signals. *Geophysical Research Letters*, *29*(23,2122) (doi 10.1029/2002GL015524).
- Ruffini, G. (1999). *OPPSCAT WP1000: Remote sensing of the ocean by bistatic radar observations: A review*. Final Report ESA Contract 13461/99/NL/GD.
- Tarantola, A. (1987). *Inverse Problem Theory*. Amsterdam, The Netherlands: Elsevier.
- Weiss, B. (2000, April). *Level 2B Data Software Interface Specification*. SeaPAC, JPL/NASA, D-16079.
- Wu, J. (1969). Froude number scaling of wind-stress coefficients. *Journal of the Atmospheric Sciences*, *26*, 408–413.
- Zavorotny, V. U. (1999, July 6). *Bistatic GPS Signal Scattering from an Ocean Surface: Theoretical Modeling and Wind Speed Retrieval from Aircraft Measurements*, talk given at the *ESA Workshop on Meteorological and Oceanographic Applications of GNSS Surface Reflections: from Modeling to User Requirements*, De Bilt, The Netherlands, <http://www.etl.noaa.gov/~vzavorotny/>.
- Zavorotny, V. U., & Voronovich, A. (2000). Scattering of GPS signals from the ocean with wind remote sensing application. *IEEE Transactions on Geoscience and Remote Sensing*, *38*(2), 951–964.